Title Page:

Mechanistic analysis of an ERK2-interacting compound that inhibits mutant-BRAF expressing melanoma cells by inducing oxidative stress

Ramon Martinez III[1], Weiliang Huang[1], Ramin Samadani, Bryan Mackowiak, Garrick Centola,

Lijia Chen, Ivie L. Conlon, Kellie Hom, Maureen A. Kane, Steven Fletcher, and Paul Shapiro*

Department of Pharmaceutical Sciences, University of Maryland-Baltimore School of Pharmacy

20 N. Penn St., Baltimore, Maryland 21201 USA

[1]Authors contributed equally

*Correspondence

a. running title: Mechanisms of a novel inhibitor of active ERK1/2 signaling.

b.   Paul Shapiro

20 Penn St., Room 561, Baltimore, MD 21201

Telephone: 410-706-8522

FAX: 410-706-5017

Email: pshapiro@rx.umaryland.edu

c. Number of:

Text pages: 28

Tables: 3

Figures: 6

References: 88

Number of words:

Abstract: 249

Introduction: 738

Discussion: 1470

d. Nonstandard abbreviations: ERK1/2, extracellular signal-regulated kinase-1/2; IEG,

immediate early genes; AP-1, activator protein-1; NRF2, nuclear factor erythroid 2-related factor

2; MAP3K8, mitogen-activated protein kinase kinase kinase-8; ROS, reactive oxygen species.

Abstract

Constitutively active extracellular signal-regulated kinase (ERK1/2) signaling promotes cancer cell proliferation and survival. We previously described a class of compounds containing a 1,1-dioxido-2,5-dihydrothiophen-3-yl 4-benzenesulfonate scaffold that targeted ERK2 substrate docking sites and selectively inhibited ERK1/2-dependent functions, including activator protein-1 (AP-1)-mediated transcription, and growth of cancer cells containing active ERK1/2 due to mutations in Ras G-proteins or BRAF kinase. The current study identified chemical features required for biological activity and global effects on gene and protein levels in A375 melanoma cells containing mutant BRAF (V600E). STD-NMR and mass spectrometry analyses revealed interactions between a lead compound (**SF-3-030**) and ERK2 including the formation of a covalent adduct on cysteine 252 located near the docking site for ERK, FXF (DEF) motif for substrate recruitment. Cells treated with **SF-3-030** showed rapid changes in immediate early gene (IEG) levels including DEF motif containing ERK1/2 substrates in the Fos family. Analysis of transcriptome and proteome changes showed that the **SF-3-030** effects overlapped with ATP-competitive or catalytic site inhibitors of MEK1/2 or ERK1/2. Like other ERK1/2 pathway inhibitors, **SF-3-030** induced reactive oxygen species (ROS) and genes associated with oxidative stress, including nuclear factor erythroid 2-related factor 2 (NRF2). Whereas the addition of the ROS inhibitor N-acetyl cysteine reversed **SF-3-030** induced ROS and inhibition of A375 cell proliferation, the addition of NRF2 inhibitors have little effect on cell proliferation. These studies provide mechanistic information on a novel chemical scaffold that selectively regulates ERK1/2-targeted transcription factors and inhibits the proliferation of A375 melanoma cells through a ROS-dependent mechanism.

3

Significance Statement

Constitutive activation of the extracellular signal-regulated kinase (ERK1/2) pathway drives the

proliferation and survival of many cancer cell types. Given the diversity of cellular functions

regulated by ERK1/2, the current studies have examined the mechanism of a novel chemical

scaffold that targets ERK2 near a substrate binding site and inhibits select ERK functions. Using

transcriptomic and proteomic analyses, we provide a mechanistic basis for how this class of

compounds inhibits melanoma cells containing mutated BRAF and active ERK1/2.

Introduction

De-regulated protein kinase activity that promotes cell proliferation and survival is a hallmark of many cancers. Thus, targeted inhibition of protein kinases with small molecules have become an important therapeutic strategy to treat cancer (Wu et al., 2016). The extracellular signal-regulated kinase-1 and 2 (ERK1/2) proteins are members of the mitogen activated protein kinase (MAPK) family and major regulators of intracellular signaling events that provide cells with a proliferation and survival advantage. Constitutive activation of ERK1/2 occurs through mutations or elevated expression of upstream activators, including receptor tyrosine kinases (RTKs), Ras G-proteins, and Raf kinases (Mendelsohn and Baselga, 2006; Bennasroune et al., 2004; Reuter et al., 2000; Shapiro, 2002; Arora and Scholar, 2005). Activating mutations in MEK1, a direct activator of the ERK1/2 proteins, may contribute to de-regulated ERK1/2 activity (Emery et al., 2009). In addition, activating mutations in a conserved glutamate in a region of ERK2 associated with protein-protein interactions are associated with the progression of cutaneous T-cell lymphomas (Mahalingam et al., 2008; da Silva Almeida et al., 2015; Arvind et al., 2005). A number of small molecular weight anti-cancer drugs targeting the ATP binding or catalytic sites on RTKs, BRAF, and MEK1/2 are being used in the clinic to block ERK1/2 signaling (Flaherty and McArthur, 2010; Zhong and Bowen, 2011; Wu et al., 2015). Despite promising initial responses, resistance to these kinase inhibitors is often observed and subsequent therapeutic options are limited. Drug resistance occurs through several mechanisms, including acquired mutations in the kinase catalytic site targeted by the compounds, activation of alternative mechanisms to turn on proteins downstream of the targeted kinase, or increases in compensatory signaling pathways that provide a survival advantage independent of the kinase being targeted (Poulikakos and Solit, 2011; Poulikakos and Rosen, 2011; Fedorenko et al., 2015;

5

Tuma, 2011). Recent efforts aimed at overcoming inherent or acquired resistance to existing

kinase inhibitors are directly targeting ERK1/2 proteins (Morris et al., 2013; Maik-Rachline and

Seger, 2016; Germann et al., 2017) and highlight the need to identify alternative approaches to

inhibit constitutively active kinase signaling pathways that promote drug resistance and drive the

survival of cancer cells.

Using computational modeling and biological testing, we have previously identified small

molecules that are designed to selectively inhibit ERK1/2 signaling by disrupting specific

substrate interactions (Samadani et al., 2015; Hancock et al., 2005; Chen et al., 2006; Boston et

al., 2011). This approach targeted two defined substrate docking sites on ERK2; the D-

recruitment site (DRS) or F-recruitment site (FRS) that interact with substrates containing D-

domains or DEF motifs, respectively (Burkhard et al., 2011; Lee et al., 2011; Sammons et al.,

2019). Previous studies suggest that most ERK1/2 substrates contain D-domains, although some

substrates, such as the ternary complex factor Elk-1, contain both a D-domain and a DEF motif

(von Kriegsheim et al., 2009). Several transcription factors that promote cancer cell growth,

including c-Myc and Fos family proteins contain the DEF motif, which is characterized by a

phenylalanine-any amino acid-phenylalanine (FXF) sequence that is 6-10 amino acids away

from the serine or threonine phosphorylation site. Hydrophobic interactions between the FXF

motif and the recruitment site on ERK1/2 facilitate kinase-substrate interactions necessary for

efficient phosphoryl transfer. To selectively target DEF motif containing transcription factors

that promote tumor growth, we previously described the identification of a class of compounds

containing a 1,1-dioxido-2,5-dihydrothiophen-3-yl 4-benzenesulfonate scaffold that inhibited

DEF motif containing substrates of the activator protein-1 (AP-1) family (Samadani et al., 2015).

This class of compounds selectively inhibited the proliferation of melanoma cells harboring

BRAF mutations and constitutively active ERK1/2. These compounds were also effective at inhibiting melanoma cell lines that are inherently resistant to clinically relevant inhibitors of mutated BRAF due to elevated mitogen-activated protein kinase kinase kinase-8 (MAP3K8) (Samadani et al., 2015).

To define the structure activity relationship for the 1,1-dioxido-2,5-dihydrothiophen-3-yl 4-benzenesulfonate-based compounds, the current studies synthesized several analogues and identified a single double bond in the sulfur heterocycle that was essential for the compound's biological activity. The findings also demonstrate that this class of compounds forms a covalent interaction with ERK2 near the FRS and have differential effects on the expression levels of ERK1/2-regulated transcription factors containing DEF motifs. The most active compound, **SF-3-030**, was examined for global effects on gene and protein levels to evaluate ERK1/2-dependent and independent mechanisms of action. The findings support a mechanism by which **SF-3-030** induced an oxidative stress response that mediated the inhibition of melanoma cells containing mutated and constitutively active BRAF.

Materials and Methods

Compound synthesis: All reactions were performed in oven-dried glassware under an inert (N_2) atmosphere. Anhydrous solvents were used as supplied without further purification. Chemicals were purchased from Sigma-Aldrich (St. Louis, MO), Alfa Aesar (Ward Hill, MA), or Oakwood Chemicals (West Columbia, SC). Reactions were monitored by thin-layer chromatography (TLC), visualizing with $KMnO_4$ stain and/or UV as appropriate. Silica gel flash column chromatography was performed with 60Å, 230-400 mesh silica gel, and crude reaction mixtures were first adsorbed onto silica gel from CH_2Cl_2 at room temperature (RT). ^1H and ^{13}C NMR spectra were recorded on a Varian 400 MHz NMR spectrometer (Bruker amaZon X) at 25 °C. Chemical shifts are reported in parts per million (ppm) and are referenced to residual non-deuterated solvent peak ($CHCl_3$: δ_H 7.26, δ_C 77.2; DMSO: δ_H 2.50, δ_C 39.5). Prior to biological testing, final compounds were confirmed to be >95% pure by HPLC chromatography. Detailed methods of the chemical synthesis are provided in the supplemental data.

Chemicals and antibodies: The MEK1/2 inhibitor AZD6244 (Cat. No. BV-2234-5), 6-(4-bromo-2-chloroanilino)-7-fluoro-N-(2-hydroxyethoxy)-3-methylbenzimidazole-5-carboxamide), was purchased from Axxora (Farmingdale, NY). The ERK1/2 inhibitor, SCH772984 (Cat. No. S7101), ((R)-1-(2-oxo-2-(4-(4-(pyrimidin-2-yl)phenyl)piperazin-1-yl)ethyl)-N-(3-(pyridin-4-yl)-1H-indazol-5-yl)pyrrolidine-3-carboxamide) was purchased from Selleckchem (Houston, TX). Antioxidants N-acetyl L-cysteine (NAC) (Cat. No. A7250), sodium pyruvate (Cat. No. P2256), and mannitol (Cat. No. M4125) were purchased from Sigma Aldrich (St. Louis, MO). NRF2 inhibitors ML385 (Cat. No. SML 1833) and Brusatol (Cat. No. SML 1868) were purchased from Sigma Aldrich. Antibodies against total c-Fos (Cat. No. 2250), FosB/B2 (Cat. No. 2251), Fra1 (Cat. No. 5281), c-Jun (Cat. No. 9165), c-Myc (Cat. No. 5605), Elk-1 (Cat. No. 9182), ß-actin

(Cat. No. 4970) and cleaved PARP (Cat. No. 9541) were purchased from Cell Signaling Technology (Beverly, MA). The phospho-specific ERK1/2 (pThr183/pTyr185)(Cat. No. M9692) and α-tubulin (Cat. No. T6074) antibodies were from Sigma Aldrich. Phosphorylation-specific antibodies against histone H3 (pSer10)(Cat. No. 9701), Elk-1 (pS383)(Cat. No. 9186), MEK1/2 (pSer217/pSer221)(Cat. No. 9121) were purchased from Cell Signaling Technology. Antibodies against ERK2 (Cat. No. sc-154), MEK 1/2 (Cat. No. sc-81504), HMOX-1 (Cat. No. sc-136960) and NRF2 (Cat. No. sc-722) were from Santa Cruz Biotechnology. A second NRF2 antibody (Cat. No. ab 137550), and the NQO1 antibody (Cat. No. ab34173) were purchased from Abcam (Cambridge, MA). The FoxD3 (Cat. No. 631701) antibody was purchased from BioLegend (San Diego CA). The OSGIN-1(Cat. No. 15248-1-AP), GCLM (Cat. No. 14241-1-AP), SRXN1 (Cat. No. 14273-1-AP), GCLC (Cat. No. 12601-1-AP), AKR1B10 (Cat. No. 18252-1-AP), G6PD (Cat. No. 66373-1-Ig), and TXNRD1 antibodies (Cat. No. 11117-1-AP) were purchased from ProteinTech (Rosemont, IL). The xCT antibody (Cat. No. NB300-317SS) was purchased from Novus Biologicals (Centennial, CO).

Cell lines: Cell lines used included HeLa cervical carcinoma cells, Jurkat T-cell leukemia cells, and NRas mutated promyelocytic leukemia HL-60 cells. Melanoma cell lines tested included A375 and SK-Mel-28 (homozygous BRAF V600E mutation), SK-MEL-5 (heterozygous BRAF V600E mutation), SK-Mel-2 (BRAF wild type, NRas Q61R mutation), and RPMI-7951 cells (heterozygous BRaf mutation), which are inherently resistant to BRAF inhibitors due to elevated MAP3K8 (Johannessen et al., 2010). Cells were purchased from American Type Culture Collection (ATCC; Manassas, VA) and grown in DMEM or EMEM plus 10% FBS. All media were supplemented with penicillin and streptomycin. The cell lines have been authenticated by evaluating short tandem repeat DNA profiles and matching with the ATCC database. Cell lines

are routinely tested for mycoplasma contamination using the MycoAlert® detection kit (Lonza; Walkersville, MD).

Cell viability/apoptosis assays: Cells were seeded at 5,000 cells/well in 96-well plates, cultured overnight, and treated for 48 hours with the indicated dose of compounds. IC_{50} values were determined using 9 data points and 3 fold dilutions of 0.001 – 10 μM for AZD6244 and SCH772984 or 0.1 – 100 μM for **SF-3-030**. Cell viability was measured according to manufacturer's instructions using the fluorescent CellTiter Blue® Assay (Promega; Madison, WI) or the CellTiter-Glo® Luminescent Cell Viability Assay (Promega; Madison, WI). To determine the minimal exposure time needed to induce an apoptotic response, cells were exposed to test compounds for various times (0-24 hours), the cells were washed, and then fresh medium was added without test compound for a total of 24 hours. Relative apoptosis was measured by immunoblotting for the cleaved form of poly (ADP-ribose) polymerase (PARP).

Reactive oxygen species measurements: Reactive oxygen species (ROS) were measured using the cell-permeable fluorogenic reagent CellROX Deep Red according to manufacturer's instructions (Thermo Fisher Scientific; Waltham, MA). Briefly, A375 melanoma cells were seeded at 10^4 cells per well in a 96-well plate. After 24 hours, the cells were co-incubated with **SF-3-030** ± various ROS inhibitors, as well as 5 μM of CellROX Deep Red reagent for 1 hour at 37°C. Subsequently, cells were washed three times with DMEM containing no Phenol Red. Live cell fluorescence was imaged using a Nikon Eclipse Ti confocal microscope, using a 10X objective magnification. Total fluorescent intensity was obtained in triplicate wells from 4 frames of view per well (~500-1000 cells/frame) with a biological duplicate performed for each treatment condition. The mean ± standard deviations were determined using NIS-Elements analysis software.

RNAseq analysis: A375 cells were treated for 1 hour with 10 μM AZD6244 or 25 μM **SF-3-030** and total RNA was isolated (RNAeasy, Qiagen; Hilden, Germany) from treated and untreated cells in duplicate samples. Differential expression analysis was done by GENEWIZ (South Plainfield, NJ.) using Illumina Genome Analyzer and HiSeq instruments in the FastQ format as previously described (Anders et al., 2013). Data were analyzed using Ingenuity® Pathway Analysis software. Changes in expression were shown for genes with false discovery rates of < 0.05.

Immunoassays: Immunoblot analysis of protein expression, phosphorylation, and cell proliferation were done as previously described (Samadani et al., 2015). Cells were washed with cold phosphate buffered saline (PBS, pH 7.2, Invitrogen; Carlsbad, CA) and protein lysates were collected with 2X SDS-PAGE sample buffer (4% SDS, 5.7M β-mercaptoethanol, 0.2M Tris pH 6.8, 20% glycerol, 5mM EDTA) Proteins were separated by SDS-PAGE, analyzed by immunoblotting, and detected using enhanced chemiluminesence (Pierce™ ECL, Thermo Fisher Scientific). Immunoblots were quantified via densitometry using the Azure c300 Chemiluminsecent Western Blot Imaging System (Azure Biosystems, Dublin, CA, USA) for image capture and data quantified on the Image Studio™ Lite Quantification software (v5.2, Li-COR Biotechnology, Lincoln, NE, USA). Immunoassays were also performed using Wes™ Simple Western (ProteinSimple, San Jose, CA, USA). Electropherograms were quantified using Compass 225 for SW software (v3.1.7, ProteinSimple, San Jose, CA, USA) applying a Gaussian peak fit distribution for determining area under the curve.

Covalent modification analysis by high resolution liquid chromatography-tandem mass spectrometry: His-tagged ERK2 was purified from *E. coli* BL21 (DE3) cells transformed with wild type *erk2* construct using the previously described method (Burkhard et al., 2011). For

11

covalent modification analysis, *in vitro* kinase reactions containing 100 µg of purified ERK2, 1mM ATP, 1X NEBuffer™ for Protein Kinases (New England Biolabs, Ipswich, MA), and 50 µM **SF-3-030** were incubated for 2 hours at 25°C. After the reactions, ERK2 protein was desalted, reduced, alkylated and trypsinolyzed on filter as described previously (Wisniewski et al., 2009; Erde et al., 2014). Tryptic peptides were separated on a nanoACQUITY UPLC analytical column (BEH130 C18, 1.7 µm, 75 µm x 200 mm, Waters Corporation; Milford, MA) over a 165-minute linear acetonitrile gradient (3 – 40%) with 0.1 % formic acid on a Waters nano-ACQUITY UPLC system (Waters Corporation; Milford , MA) and analyzed on a coupled Thermo Scientific Orbitrap Fusion Lumos Tribrid mass spectrometer (Thermo Scientific; San Jose, CA) as described (Williamson et al., 2016). Full scans were acquired at a resolution of 120,000, and precursors were selected for fragmentation by higher-energy collisional dissociation (normalized collision energy at 32 %) for a maximum 3-second cycle. Tandem mass spectra were searched against the ERK2 protein sequence using a Sequest HT algorithm (Eng et al., 2008) and a MS Amanda algorithm (Dorfer et al., 2014) with a maximum precursor mass error tolerance of 10 ppm. Possible substitution (S_N2' and S_N2, +115.9932), Michael addition (+324.0126) and carbamidomethylation of cysteine were treated as dynamic modifications. Resulting hits were validated at a maximum false discovery rate of 0.01 using a semi-supervised machine learning algorithm Percolator (Kall et al., 2007). The probabilities of modification sites were computed using a ptmRS algorithm (Taus et al., 2011).

Saturation Transfer Difference-Nuclear Magnetic Resonance (STD-NMR) analysis: STD-NMR analysis of ligand binding to ERK2 as was done previously described for p38 MAP kinases (Shah et al., 2017). A 1 mM stock solution of **SF-3-030** was made in 85% D_2O:15% d6-DMSO (v/v). STD-NMR samples contained 150 mM NaCl, 50 mM phosphate (pH 7), 200 µM

SF-3-030, and 5 μM ERK2 protein in D_2O. Spectra of both compound and ligand bound protein were recorded on an Agilent DD2 500-MHz spectrometer equipped with a 5-mm inverse proton–fluorine–carbon–nitrogen probe head at 25°C. Further detailed methods of the NMR protocol used are provided in the supplemental data.

Differential protein expression by high-resolution liquid chromatography tandem mass spectrometry: A375 cells grown on 10 cm plates were treated for 4 and 12 hours with 0.1% DMSO vehicle, 25 μM **SF-3-030** or 10 μM SCH772984. Following one wash in cold PBS, the cells were collected by scraping twice with cold PBS, centrifuged at 3000 rpm for 2 min. and the cell pellets were stored at -80°C. Cells were lysed in 4 % sodium deoxycholate, reduced, alkylated and trypsinolyzed on filter as described (Wisniewski et al., 2009). Tryptic peptides were separated on a nanoACQUITY UPLC analytical column (CSH130 C18, 1.7 μm, 75 μm x 200 mm, Waters Corporation; Milford, MA) over a 180 min linear acetonitrile gradient (3 – 43%) with 0.1 % formic acid on a Waters nano-ACQUITY UPLC system (Waters Corporation; Milford, MA), and analyzed on a coupled Thermo Scientific Orbitrap Fusion Tribrid mass spectrometer (Thermo Scientific; San Jose, CA) as described (Williamson et al., 2016). Full scans were acquired at a resolution of 120,000 and precursors were selected for fragmentation by higher-energy collisional dissociation (normalized collision energy at 30%) for a maximum 3-second cycle. Tandem mass spectra were searched against a UniProt human reference proteome using a SEQUEST HT algorithm (Eng et al., 2008) with a maximum precursor mass error tolerance of 10 ppm. Resulting hits were validated at a maximum false discovery rate of 0.01 using a semi-supervised machine learning algorithm Percolator (Kall et al., 2007). Abundance ratios were measured by comparing the MS1 peak volumes of peptide ions, whose identities were confirmed by MS2 sequencing as described above. Label-free quantifications were

13

performed using an aligned AMRT (Accurate Mass and Retention Time) cluster quantification algorithm (Qi et al., 2012). Pathway and gene ontology analysis were performed with Qiagen Ingenuity and Panther GO databases, as described (Kramer et al., 2014; Mi et al., 2017). Proteins showing at least a doubling in expression as compared to untreated cells, with an FDR adjusted ANOVA p-value <0.05, were considered significantly changed and used for further analysis. FDR corrected Fisher's exact p-values of < 0.05 using a previously described procedure for multiple testing were used in the gene ontology analyses to identify biological processes, molecular functions, and cellular components associated with observed protein changes (Hochberg, 1995). Ingenuity pathway database was used to predict canonical pathways and upstream regulators according to the proteins that were significantly different using an absolute activation z-score of > 2 for at least one condition with a Fisher's exact test p-value < 0.05.

Lactate dehydrogenase (LDH)/cytotoxicity assay: Cells were seeded 5,000 cells/well in 96-well plates, cultured overnight, and treated for 48 hours with the indicated dose of compound SF-3-030. Cytotoxicity via LDH release was measured according to manufacturer's instructions using the CyQUANT™ LDH Cytotoxicity Assay Kit (Thermo Fisher Scientific: Waltham, MA).

Statistical analysis: Graphical statistical analysis was performed using a one-tailed ANOVA with a 95% confidence interval using GraphPad-Prism V.5.01. Three biological replicates were chosen for data subjected to statistical analysis. The data represent descriptive statistics and were used to summarize key findings. Results were considered statistically significant if the p-value is less than 0.05.

Results

The double bond in the sulfur heterocycle is required for biological activity. Our previous studies described a novel class of small molecules containing a 1,1-dioxido-2,5-dihydrothiophen-3-yl 4-benzenesulfonate scaffold that selectively inhibited BRAF mutated melanoma cells containing constitutively active ERK1/2 signaling (Samadani et al., 2015). A limited structure-activity relationship study was performed to determine key chemical features required for the compound's biological activity. Modifications of the parent compound, **SF-3-026**, focused on the benzene ring, the linker region connecting the two ring structures, and removal of the double bond in the sulfur heterocycle (Fig. 1). The analogues were tested at a single high dose for effects on viability of cancer cell lines containing BRAF mutations (A375, RPMI-7951, and SK-Mel-28), NRas mutation (HL60), or no known mutations in ERK1/2 pathway proteins (HeLa and Jurkat) (Fig. 1). RPMI-7951 cells are inherently resistant to BRAF targeted inhibitors due to upregulated expression of MAP3K8 (Johannessen et al., 2010). In agreement with our previous studies (Samadani et al., 2015), **SF-3-026**, **SF-3-027**, **SF-3-029**, and **SF-3-030** showed selective inhibition of cancer cell lines with activating mutations in the ERK1/2 pathway (Fig. 1). The inhibitory effects were lost in compounds where the double bond in the sulfur heterocycle was removed (Fig. 1). Select modifications to the benzene group or linker in the absence of the double bond in the sulfur heterocycle had no effect on cell viability indicating the 1,1-dioxido-2,5-dihydrothiophen-3-yl moiety was essential for the compound's biological activity (Fig. 1).

Previous studies showed that catalytic site inhibitors of MEK1/2 and ERK1/2 are selective for cells with activating BRAF or Ras mutations (Yeh et al., 2007; Morris et al., 2013). Similarly, we determined the IC_{50} values for **SF-3-030** and ATP dependent/catalytic site inhibitors of MEK1/2 and ERK1/2 in four cancer cell lines and show that all compounds favored

16

inhibition of cells containing activating BRAF and Ras mutations (Supplemental Table 1). The reported doubling times for A375, HeLa, and Jurkat cells are ~25-30 hours compared to ~50 hours for the RPMI-7951 cells indicating that each compound's potency is independent of cell growth rates. These findings provide additional support that **SF-3-030** inhibitory effects on cell growth are correlated with ERK1/2 activity.

The effects of **SF-2-110** (inactive control), **SF-3-026**, and **SF-3-030** (Supplemental Fig. 1A) on cell viability were further evaluated in dose – response assays using four melanoma cell lines containing either BRAF or NRas mutations. As expected, **SF-2-110** did not affect the viability of any of the cell lines up to 50 μM (Supplemental Figs. 1B-E). In contrast, **SF-3-026** and **SF-3-030** inhibited all cell lines with IC$_{50}$ values in the 5-10 μM range with **SF-3-030** showing the highest potency against SK-MEL-28 and SK-MEL-2 cells (Supplemental Figs. 1B-E). These findings indicate that the sensitivity of cancer cells *in vitro* to the lead compounds is independent of the BRAF or NRas mutational status.

SF-3-030 directly interacts with ERK2 through non-covalent and covalent mechanisms. Given the higher inhibitory potency of **SF-3-030**, we evaluated whether this compound directly interacted with ERK2. Using Saturation Transfer Difference-Nuclear Magnetic Resonance (STD-NMR), it was confirmed that **SF-3-030** interactions with ERK2 occur primarily through a reversible interaction of the naphthalene group and the sulfur heterocycle (Supplement Fig. 2). However, the requirement for the double bond in the sulfur heterocycle of **SF-3-030** for biological activity suggested that the compound's mechanism of action involves the formation of covalent adducts with cysteine residues. Two possible **SF-3-030** adducts could result from a Michael addition or a substitution reaction that would increase the molecular weight of a cysteine by 324 or 116 Da, respectively (Fig. 2A). To test this, ERK2 was incubated with **SF-3-030** and

17

covalent adducts were analyzed by high-resolution liquid chromatography-tandem mass spectrometry. Of the seven cysteine residues in ERK2, cysteine 252 (C252) was the predominant residue modified by a 116 Da mass, suggesting a substitution reaction and decomposition of **SF-3-030** (Fig. 2A/B & Supplemental Figure 3). C252 is located near the DEF-motif recruitment site, which is consistent with its proposed mechanism of targeting DEF motif containing substrates (Samadani et al., 2015). Other major MAP kinases such as p38α and JNK1 do not have a cysteine located at this site. We have also previously determined that **SF-3-030** had no effect on p38 MAP kinase signaling (Samadani et al., 2015), suggesting that **SF-3-030** is not acting as a random alkylating agent or affecting similar MAP kinases. These data suggest that the initial binding interactions of **SF-3-030** with ERK2 involve non-covalent interactions that position the compound to form a covalent bond between C252 and the sulfur heterocycle group.

SF-3-030 selectively regulates ERK-dependent immediate early gene expression. We next examined relative protein levels of ERK1/2-regulated immediate early genes (IEG). Previously, we showed that a 1 hour treatment with **SF-3-030** caused differential changes in AP-1 protein levels characterized by inhibition of Fra-1, FosB, and the alternative splice variant FosB2 but no effect on c-Fos levels (Samadani et al., 2015). The relative levels of these proteins along with other AP-1 members were examined in A375 cells treated for 0-24 hours with **SF-3-030** or the ERK1/2 catalytic site inhibitor SCH772984 as a positive control. Similar to our previous studies (Samadani et al., 2015), a 1 hour treatment with **SF-3-030** or SCH772984 had little effect on c-Fos levels (Fig. 3A). However, after 2 hours treatment, c-Fos increased only with **SF-3-030** and persisted for up to 24 hours (Fig. 3A). Another major component of the AP-1 complex, c-Jun, increased with either **SF-3-030** or SCH772984 treatments (Fig. 3A). It should be noted that the increased levels of c-Fos and c-Jun do not correlate with increased AP-1 activity, which we've

shown to be inhibited in these and other cell lines treated with **SF-3-030** (Samadani et al., 2015; Defnet et al., 2019b).

Other Fos family members, including FosB/B2 and Fra-1 decreased in cells treated with SCH772984 (Fig. 3A). Cells treated with **SF-3-030** also showed decrease Fra-1 levels whereas FosB/B2 levels transiently decreased followed by an increased after 4 hours as observed with c-Fos (Fig. 3A). The levels of c-Myc, a potential target for treating melanoma (Polsky and Cordon-Cardo, 2003; Korkut et al., 2015), showed a rapid inhibition by **SF-3-030** when compared to SCH772984 (Fig. 3A). Interestingly, c-Myc levels increased back to basal levels after 24 hour treatment with **SF-3-030** (Fig. 3A). However, this dose of **SF-3-030** is lethal to ~90% of A375 cells after 48 hours exposure (Supplement Fig. 1B). A transient increase in the ERK1/2-mediated phosphorylation of Elk-1, a ternary complex factor involved in regulating *c-fos* and other IEG (Shaw and Saxton, 2003), was observed in **SF-3-030** treated cells and correlated with ERK1/2 phosphorylation (Fig. 3B). However, there was no evidence that MEK1/2, the upstream activator of ERK1/2, was activated indicating **SF-3-030** was acting at the level of ERK1/2 (Supplemental Fig. 4).

The dose-dependent effect of the active compounds **SF-3-026** and **SF-3-030** on IEG levels were examined after a 4 hour exposure. The inactive control, **SF-2-110**, had no effect on c-Fos, c-Jun, Fra-1, FosB/B2, or c-Myc levels (Fig. 3C). In contrast, **SF-3-026** and **SF-3-030** caused a dose-dependent decrease in Fra-1, FosB/B2, and c-Myc protein levels but an increase in c-Jun and c-Fos (Fig. 3C). The increased potency of **SF-3-030** in affecting IEG protein levels compared to the parent compound **SF-3-026** is consistent with our previous studies (Samadani et al., 2015). It is also noted that **SF-3-030** at a dose near its IC_{50} (~5 μM) for inhibition of cell proliferation was as potent at inhibiting Fra-1 and c-Myc protein levels as the 5 μM doses of

AZD6244 or SCH77294 (Fig. 3C). Quantitative analysis of c-Fos, Fra-1, and c-Myc protein levels after exposure with 25μM **SF-2-110** or **SF-3-030** is shown in Figure 3D. Together, these findings demonstrate that the lead compounds can differentially affect ERK1/2-regulated transcription factors.

It was next determined whether the changes in IEG expression observed after 1-2 hours with **SF-3-030** (Fig. 3A) coincided with the exposure time needed to induce an apoptotic response. In these experiments, A375 cells were exposed to **SF-3-030** for various times, washed to remove excess compound, and then incubated with serum-supplemented growth medium for a total of 24 hrs. Apoptosis was evident after 2 hours exposure to **SF-3-030** as measure by the appearance of cleaved PARP (Fig. 3E). This exposure time also coincided with the loss of histone H3 phosphorylation at Ser10, which is a marker of mitosis and is observed during the transcription of selective IEGs in response to ERK1/2 pathway activation (Sassone-Corsi et al., 1999). Loss of histone H3 phosphorylation after 2 hours exposure to **SF-3-030** suggests that mitotic progression is inhibited and that phosphorylation of S10 is dispensable for regulating the transcription of IEG, such as c-Fos and c-Jun as previously reported (Drobic et al., 2010).

SF-3-030 regulates ERK1/2-dependent and independent transcription. RNAseq analysis was used to measure early changes in gene expression patterns and identify on- and off-target effects of **SF-3-030**. Total RNA was isolated from A375 cells treated for 1 hour with an IC_{90} dose (25μM) of **SF-3-030** or the MEK inhibitor AZD6244 (10 μM) as a positive control for ERK1/2 pathway inhibition. The IC_{90} dose for **SF-3-030** was used as it was determined to have no general cytotoxicity in LDH assays (data not shown; (Defnet et al., 2019a)). Approximately 16,000 transcripts were identified in each condition and statistically significant changes (≥1.5 fold) in transcript expression between treated and untreated cells were reported. We identified 38

or 68 transcripts in cells treated with **SF-3-030** or AZD6244, respectively, which showed significant decreases with 12 genes common to both treatments (Supplemental Table 2). ERK1/2 pathway targets involved in cell growth and survival that decreased with both treatments included *c-Myc, CTGF, SOX11,* and *GATA3.* AZD6244 also inhibited transcription of *c-Fos*, *Egr-1*, and *IER3* genes, which are elevated in BRAF V600E mutated melanoma cells and may promote ERK-mediated growth of these tumor types (Pratilas et al., 2009). The inhibition of c-Myc by **SF-3-030**, AZD6244, and SCH772984 at the RNA and protein levels (Fig. 3) supports a shared mechanism of targeting ERK-mediated signaling by these compounds.

The data also revealed that AZD6244 inhibited many negative regulators of the ERK1/2 pathway, including Sprouty (*SPRY*) and dual specificity phosphatases (*DUSP*) transcripts (Supplemental Table 2). *SPRY1* was the only negative regulator of ERK1/2 signaling that was inhibited by both AZD6244 and **SF-3-030** (Supplemental Table 2). Additional growth-related genes that decreased only with AZD6244 treatment included regulators of epidermal growth factor (EGF) receptor signaling including *c-Fos*, *TGFA*, and *HBEGF* (Supplemental Table 2). In contrast, only **SF-3-030** inhibited a unique set of growth and angiogenesis promoting genes including *CYR61* (also called IGF-binding protein 10), which may promote tumor progression during hypoxia (Kunz et al., 2003), and *BCL6*, which has been associated with poor overall survival of melanoma patients (Alonso et al., 2004).

There were 14 or 24 transcripts that increased >1.5 fold following treatment with **SF-3-030** or AZD6244, respectively, relative to untreated cells, and only one gene, *CHMP4C*, was common to both treatments (Supplemental Table 2). *CHMP4C* is involved in sorting and delivery of endosomal vesicles to the lysosome and in cell cycle checkpoint control during cytokinesis (Carlton et al., 2012). Ingenuity Pathway Analysis (IPA) indicated that several genes

21

upregulated in response to **SF-3-030** treatment, including heme oxygenase-1 (*HMOX1*), *c-Fos*, *c-Jun*, and DnaJ homolog subfamily B member 1 (*DNAJB1*) (Supplemental Table 2), were consistent with activation of a nuclear factor erythroid 2-related factor 2 (*NRF2*) mediated oxidative stress response. However, given the exposure to **SF-3-030** was only 1 hour, it is likely that other transcription factors besides NRF2 are regulating these genes at this time point.

Other genes upregulated by **SF-3-030** included *MAP3K14* (also called NF-kappa-beta-inducing kinase, *NIK*), which activates NF-κB and the early growth reponse-1 (*Egr-1*) transcription factor, which may have tumor suppressor functions through regulation of p53 (Shin et al., 2006). Transcripts that increased only in response to AZD6244 treatment included *SOX2* and *FOXD3*, which are associated with survival of melanoma-initiating cells, metastasis and drug resistance (Santini et al., 2014; Abel et al., 2013). The activation status of the top 50 upstream regulators predicted to be affected following treatment with **SF-3-030** or AZD6244 was determined using IPA software. Using Z-scores of >2 or <-2 to indicate activation or inactivation, respectively, and p values of <0.03, AZD6244 predictably inhibited many regulators of ERK1/2 and other MAP kinase signaling pathways (Supplemental Table 3). In contrast, **SF-3-030** was predicted to affect only 6 regulators, including activation of EGR1 as indicated previously (Supplement Table 3). Given some overlap with AZD6244-regulated genes, these data suggest that **SF-3-030** treatment affects fewer cellular signaling events than AZD6244 and that early MAP kinase signaling events largely remain intact.

SF-3-030 enhances markers of mitochondrial dysfunction and oxidative stress. To gain further insight into the mechanism of **SF-3-030** inhibition of cell proliferation, we next used high-resolution liquid chromatography-tandem mass spectrometry to determine the changes in levels of soluble proteins in A375 cells treated for 4 or 12 hours with SCH772984 or **SF-3-030**. After 4

hours, 22 (**SF-3-030**) or 16 (SCH772984) proteins were identified that showed significant ($p<0.05$) changes compared to untreated cells (Supplemental Table 4). A summary of proteins that showed statistically significant increases or decreases (≥ 1.5 fold) with **SF-3-030** or SCH772984, as compared to untreated controls, is shown in table 1A/B. At the 4 hour time point, only one protein, adenosylhomocysteinase (AHCY), which regulates the generation of the S-adenosylmethionine methyl donor, was inhibited with **SF-3-030** or SCH772984 treatment. Proteins that increased after exposure to **SF-3-030** included the zinc finger protein 774 (ZNF774) that has recently been shown to have tumor suppressor functions in hepatocellular carcinoma (Guan et al., 2020), transcription factor 4 (TCF4), which regulates cell differentiation, and HMOX1 (Table 1A). **SF-3-030** decreased cytochrome c-type heme lyase (HCCS) levels suggesting defects in mitochondrial electron transport function (Table 1A). SCH772984 increased levels of the transmembrane and TPR repeat-containing protein 1 (TMTC1), which indicated disruption of calcium homeostasis in the endoplasmic reticulum (Sunryd et al., 2014), and decreased the tetratricopeptide repeat protein (TTC29) whose function is currently unknown (Table 1B).

After 12 hours, 44 and 48 proteins showed significant changes ($p<0.05$) with **SF-3-030** and SCH772984 treatment, respectively, as compared to untreated cells (Supplemental Table 5). Proteins that increased or decreased ≥ 1.5 fold with **SF-3-030** or SCH772984 treatments relative to untreated controls are shown in Tables 2A or B, respectively. Common to **SF-3-030** or SCH772984 treatments was increased levels of TCF4 and cytochrome c oxidase assembly protein (SCO2) and decreased levels of a protein involved in ribosome biogenesis (RSL24D1). SCO2 has been associated with p53-mediated apoptosis signaling pathways through the generation of ROS (Madan et al., 2013).

Unique to **SF-3-030** was a significant increase in the oxidative stress-induced growth inhibitor 1 (OSGIN1) protein (Table 2A), which is regulated by oxidized lipids and NRF2 during oxidative stress to promote cytochrome c release from mitochondria (Li et al., 2007). MEMO1, a protein involved in the sustained production of ROS (MacDonald et al., 2014), was also increased in cells exposed to **SF-3-030** (Tables 1A and 2A). As was observed after 4 hours, HCCS levels were also decreased after 12 hour exposure to **SF-3-030** (Tables 1A and 2A) further supporting compromised mitochondria function. Together, these findings indicate **SF-3-030** induced signaling events that reduce mitochondrial function and increase ROS. After 12 hours exposure to SCH772984 a significant induction of the Forkhead box protein D3 (FOXD3) was observed (Table 2B) and is consistent with previous studies that show upregulation of this protein promotes resistance to Raf and MEK inhibitors (Abel et al., 2013). Immunoblot analysis confirmed the induction of FOXD3 expression in A375 cells treated with SCH772984 but not in **SF-3-030** treated cells (Supplemental Fig. 5).

Based on the observed changes in protein levels, IPA pathway analysis suggested a potential role for **SF-3-030** induction of NRF2-mediated oxidative stress response and heme degradation in agreement with mitochondrial dysfunction. These findings are consistent with previous studies that implicate the ERK1/2 pathway in regulating oxidative phosphorylation in melanoma cells and the induction of ROS following treatment with inhibitors of BRAF and MEK1/2 (Haq et al., 2013; Cesi et al., 2017; Yuan et al., 2020). Immunoblot analysis confirmed that **SF-3-030** treatment rapidly induced NRF2 levels that were sustained for at least 24 hours and that NRF2 induction could be inhibited by co-treatment with the ROS inhibitor *N*-acetylcysteine (NAC) (Fig. 4A-C).

24

SF-3-030 inhibition of A375 cell proliferation is dependent on ROS induction but independent of NRF2. The transcriptome and proteome data provided evidence for the generation of ROS in cells treated with **SF-3-030**. We confirmed the increased ROS production in A375 cells after a 1 hour treatment with **SF-3-030**, which was partially inhibited by co-treatment with several ROS inhibitors (Fig. 5A). NAC was the only ROS inhibitor that restored A375 cell proliferation in the presence of **SF-3-030** (Fig. 5B). Similarly, only NAC reversed **SF-3-030** induction of c-Fos (Fig. 5C). While these data indicate that NAC may mitigate ROS production by **SF-3-030** to restore A375 cell proliferation, there was also the possibility that NAC directly forms adducts with **SF-3-030**, which would reduce the compound's effective concentration and biological activity. However, using thin layer chromatography to separate compounds, we found no evidence that NAC directly interacted with **SF-3-030** following a 1 or 24 hour incubation in both PBS and methanol solvent systems (data not shown).

Induction of NRF2 has been implicated in protecting against oxidative stress induced by anti-cancer drugs and may contribute to drug resistance (Telkoparan-Akillilar et al., 2019). To assess whether NRF2 induction protected cells from **SF-3-030** inhibition, we co-treated A375 cells with the NRF2 inhibitors, ML-385 or brusatol (Singh et al., 2016; Olayanju et al., 2015; Ren et al., 2011). **SF-3-030** and sulforaphane, as a positive control, induced NRF2 and target genes such as HMOX-1, OSGIN-1, NAD(P)H dehydrogenase [quinone] 1 (NQO1), glutamate-cysteine ligase modifier subunit (GCLM), and sulfiredoxin 1 (SRXN1) (Fig. 6A/B and Supplemental Fig. 6A). In contrast, protein levels for other NRF2-regulated genes, including aldo-keto reductase family 1 member B10 (AKR1B10), glutamate-cysteine ligase catalytic subunit (GCLC), glucose-6-phosphate dehydrogenase (G6PD), cystine/glutamate transporter/solute carrier family 7 member

25

11 (xCT/SLC7A11), and thioredoxin reductase 1 (TXNRD1) were not induced by **SF-3-030** (Supplemental Fig. 7).

As compared to sulforaphane, **SF-3-030** induced a more robust and sustained induction of HMOX-1 indicating qualitative differences in NRF2 activators. Brusatol was a potent inhibitor of **SF-3-030** or sulforaphane induction of NRF2 and its target genes. Although ML-385 inhibited HMOX-1 induced by sulforaphane after 24 hours (supplemental Fig. 6A/B), it was not as effective as brusatol at inhibiting NRF2 signaling induced by **SF-3-030** (Fig. 6A). ML-385 had no effect on cell proliferation up to 50 μM, however brusatol inhibited A375 cells in a dose dependent manner (Fig. 6 C/D). Co-treatment with brusatol or ML-385 had little effect on **SF-3-030** or sulforaphane inhibition of A375 cell proliferation, indicating NRF2 induction was dispensable for the cell response to these compounds (Fig. 6E/F, supplement Fig. 6C/D). Dose-dependent inhibition of A375 cells by sulforaphane or brusatol alone supports the high sensitivity these cells have to fluctuations in ROS (Meierjohann, 2014). Together, these data indicate that **SF-3-030**-mediated inhibition of A375 melanoma cell proliferation is through a mechanism that is ROS-dependent, and NRF2-independent.

Discussion

The first objective of the current studies was to elucidate the structure activity relationship of a 1,1-dioxido-2,5-dihydrothiophen-3-yl 4-benzenesulfonate chemical scaffold that we previously identified to selectively inhibit cancer cells containing activated ERK1/2 signaling (Samadani et al., 2015). The dependence on a double bond in the sulfur heterocycle for biological activity indicated the compound's mechanism of action involved the formation of covalent adducts with cysteine residues on ERK1/2 and perhaps other proteins through Michael addition chemistry. **SF-3-030** was confirmed via STD-NMR and mass spectrometry-based analyses to interact with ERK2 via non-covalent interactions and the formation of a covalent adduct on C252 near the FRS. While the formation of covalent adducts raises the concern about specificity and off-target effects, we have found no evidence that **SF-3-030** leads to changes in other MAP kinase signaling pathways or randomly interacts with cysteine using the ROS inhibitor NAC (data not shown). This indicates that the chemical structure of **SF-3-030** confers target selectivity and prevents random interactions with sulfhydryl groups.

There is the potential that **SF-3-030** forms a covalent adduct with KEAP1 the negative regulator of NRF2. KEAP1 has up to 21 cysteine residues that may be modified by chemical stressors to relieve KEAP1 inhibition and allow NRF2 activation (Dayalan Naidu and Dinkova-Kostova, 2020). Sulforaphane, which modifies KEAP1 on C151 to activate NRF2, showed qualitative differences in the expression of NRF2-regulated genes as compared to **SF-3-030** (Fig. 6 and supplemental Fig. 6). It will be interesting to evaluate whether **SF-3-030** also modifies KEAP1 cysteine residues and how they impact NRF2 functions. As indicated in the current studies, **SF-3-030** induction of NRF2 did not appear to affect A375 cell proliferative responses to **SF-3-030**.

Despite past concerns about safety and off-target toxicity, advances in structure function relationships and medicinal chemistry have generated renewed interest in the development of irreversible binding drugs for treating disease (Singh et al., 2011). There are several small molecule anti-cancer drugs in the clinic that form covalent adducts on receptor and non-receptor tyrosine kinases through Michael addition (reviewed in (Zhao and Bourne, 2018)). Afatinib, osimertinib, and neratinib form irreversible adducts on cysteine residues in the catalytic sites of EGF receptors for the treatment of non-small cell lung cancers and breast cancers while ibrutinib targets Bruton's tyrosine kinase (BTK) for the treatment of lymphoma/leukemia. Additionally, there is renewed interest in targeting ERK1/2 with small molecules via allosteric inhibition of substrate interactions sites, such as the D-recruitment site (DRS) (Sammons et al., 2019). Recent studies have identified a small molecule inhibitor that covalently binds to a conserved cysteine (C159) in the DRS of ERK2 (Kaoud et al., 2019). This compound selectively blocked the activation of ERK1/2, did not modify other members of the MAP kinase family, and inhibited the proliferation of melanoma cells with BRAF (V600E) mutations that were resistant to BRAF inhibitors (Kaoud et al., 2019). Future studies will be aimed at identifying if cysteine residues on other proteins may be modified by **SF-3-030** to establish their role in cell signaling and growth inhibition.

The second objective of the studies was to evaluate global effects of **SF-3-030** on gene and protein changes to gain insight into this chemical scaffold's mechanism of action. The transcriptome and proteome data show that the overall number of genes and proteins affected by the lead compound, **SF-3-030**, are less than or similar to the number of proteins targeted by known ERK1/2 or MEK1/2 ATP competitive or catalytic site inhibitors. Similar to the ATP-competitive ERK1/2 pathway inhibitors, **SF-3-030** appears to be more selective for cancer cells

containing constitutively activating ERK1/2 pathway mutations. While rapidly dividing cells are typically more sensitive to anti-cancer drugs, **SF-3-030** effects on a select number of cells with activating ERK1/2 pathway mutations were shown to be independent of cell doubling times. Although further studies with additional cell lines will be needed to verify this observation, these data indicate that off-target effects on non-transformed cells may be limited.

Transcriptome and proteome analyses indicated that **SF-3-030** induced rapid changes in the levels of ERK1/2 regulated transcription factors consistent with an oxidative stress response. Transcription factors such as c-Fos and c-Jun are elevated in response to oxidative or metabolic stress (Webster et al., 1994) and ROS-mediated induction of ERK1/2 can enhance Elk-1 mediated transcription and c-Fos expression (Muller et al., 1997). It was intriguing that **SF-3-030** caused a robust induction of c-Fos but inhibited c-Myc protein levels (Fig. 3) and that these changes occurred at the level of transcription (Supplemental Table 2). Other examples where proteins levels increase due to **SF-3-030** induction of transcription include c-Jun and HMOX1. In contrast, **SF-3-030** also inhibited Fra-1 levels but there was no evidence this occurred through effects on transcription (Fig. 3 and Supplemental Table 2). It is possible that the 1 hour time point used to evaluate transcriptome changes by RNAseq did not capture changes in Fra-1 transcription. The expression of Fra-1 and other Fos family proteins are regulated by c-Fos and subsequent AP-1 complex activity (Milde-Langosch, 2005). However, c-Fos induction in the current studies does not correlate with increased AP-1 activity, which we previously showed to be inhibited by **SF-3-030** (Samadani et al., 2015; Defnet et al., 2019a). While apoptosis can be induced by c-Fos induction (Preston et al., 1996), further studies will be needed to clarify the requirement for c-Fos expression in **SF-3-030** mediated cell death in the absence of AP-1 activity.

29

ERK1/2 activation increases the expression of c-Myc (Kerkhoff et al., 1998), which can protect melanoma cells against oxidative stress (Benassi et al., 2006). In contrast, **SF-3-030** mediated downregulation of c-Myc and its potential role in responding to elevated ROS by regulating the synthesis of antioxidants such as glutathione (Gao et al., 2009). Following exogenous hydrogen peroxide-induced oxidative stress, ERK1/2 phosphorylation of c-Myc at serine 62 facilitates c-Myc recruitment to the glutamate-cysteine ligase catalytic subunit (GCLC) promoter and the expression of GCLC, the rate limiting enzyme involved in glutathione synthesis (Benassi et al., 2006). However, in the current studies, the dramatic inhibition of c-Myc protein levels by **SF-3-030** after 8 hours (Fig. 3A) is not observed with GCLC (Supplement Fig. 7). Nonetheless, targeted inhibition of c-Myc with ERK1/2 pathway inhibitors is a suggested approach to decrease the proliferation of melanoma cells and overcome drug resistance (Ciuffreda et al., 2009; Korkut et al., 2015).

The role of reactive oxygen species (ROS) in promoting or inhibiting cancer cells is subject to debate and there is evidence to support that either increased or decreased ROS production can sensitize cancer cells to growth inhibition and cell death (Trachootham et al., 2009; Galadari et al., 2017). While the use of anti-oxidant strategies may protect against some cancers (Trachootham et al., 2009), there are limited clinical data that supports the beneficial effects of using anti-oxidant supplements to reduce the risk of developing cancer (Goodman et al., 2011). However, the mechanisms used by many anti-cancer drugs to kill cells involves increased oxidative stress (Trachootham et al., 2009). Melanocytes and melanoma cells are particularly sensitive to ROS and the ROS dose will likely determine whether cells are able to adapt or will die (Meierjohann, 2014), Additional evidence supports the use of oxidative stress to inhibit melanoma cell metastasis (Piskounova et al., 2015). While ROS activation may not be sufficient

30

to inhibit all cancer cells, enhanced ROS production may also play a role in improving anti-cancer efficacy of combination therapies (Adams et al., 2013). Recent data suggests that therapeutic approaches that increased ROS may be beneficial to patients who have developed resistance to BRAF and MEK1/2 inhibitors (Wang et al., 2018).

The selectivity of **SF-3-030** towards cancer cells with activating ERK1/2 pathway mutations supports the idea that exploiting ROS homeostasis may be therapeutically beneficial in some cancers. While upregulation of ROS may provide a survival advantage in melanomas that are resistant to ERK1/2 pathway inhibitors, additional increases in ROS with histone deacetylase (HDAC) inhibitors promoted an apoptotic response in these cells (Wang et al., 2018). Further studies will be needed to determine whether **SF-3-030** induces DNA instability and ROS production like HDAC inhibitors. DNA damage may induce the ROS-responsive tumor suppressor OSGIN1 protein to enhance apoptosis in osteosarcoma cells through a mechanism involving p53 disruption of mitochondria functions and cytochrome c release (Hu et al., 2012). Although **SF-3-030** induced the protein levels of OSGIN1 and a subset of NRF2-regulated genes (Fig. 6A/B), the NRF2 inhibitor brusatol did not affect **SF-3-030** inhibition of A375 cell proliferation (Fig. 6F). These findings raise the potential to develop ROS activators that are lethal to cancer cells but do not promote a NRF2 response that leads to chemoresistance and cancer cell survival (Okazaki et al., 2020). Taken together, the current studies provide mechanistic support to evaluate how ROS production by **SF-3-030** and related compounds can be used as an approach to inhibit the proliferation of cancers cells with activating mutations in the ERK1/2 pathway.

31

Acknowledgements

The work was supported by NIH grants R01 CA120215 (PS, ADM) and F31 GM100693 (RS) and by the University of Maryland Computer-Aided Drug Design Center. In addition, support was provided in part by the University of Maryland Baltimore, School of Pharmacy Mass Spectrometry Center (SOP1841-IQB2014). This study made use of NMRbox: National Center for Biomolecular NMR Data Processing and Analysis, a Biomedical Technology Research Resource (BTRR), which is supported by NIH grant P41GM111135. Training support was provided by an NIH T32 grant (NIGMS T32 GM066706) and by an NIGMS Initiative for Maximizing Student Development Grant (2 R25-GM55036). We thank Jacob Scheenstra for technical assistance.

Author Contributions

Participated in research design: Martinez, Huang, Samadani, Fletcher, Kane, and Shapiro.

Conducted experiments: Martinez, Huang, Hom, Chen, Centola, and Samadani,

Contributed new reagents or analytic tools: Fletcher, Chen, and Conlon.

Performed data analysis: Huang, Martinez, Hom, Mackowiak, Centola, Samadani, and Shapiro.

Wrote or contributed to the writing of the manuscript: Huang, Martinez, Hom, Kane, Fletcher, and Shapiro.

References

Abel, E. V., K. J. Basile, C. H. Kugel, 3rd, A. K. Witkiewicz, K. Le, R. K. Amaravadi, G. C. Karakousis, X. Xu, W. Xu, L. M. Schuchter, J. B. Lee, A. Ertel, P. Fortina, and A. E. Aplin. (2013) Melanoma adapts to RAF/MEK inhibitors through FOXD3-mediated upregulation of ERBB3. J Clin Invest. 123: 2155-68.

Adams, D. J., Z. V. Boskovic, J. R. Theriault, A. J. Wang, A. M. Stern, B. K. Wagner, A. F. Shamji, and S. L. Schreiber. (2013) Discovery of small-molecule enhancers of reactive oxygen species that are nontoxic or cause genotype-selective cell death. ACS Chem Biol. 8: 923-9.

Alonso, S. R., P. Ortiz, M. Pollan, B. Perez-Gomez, L. Sanchez, M. J. Acuna, R. Pajares, F. J. Martinez-Tello, C. M. Hortelano, M. A. Piris, and J. L. Rodriguez-Peralto. (2004) Progression in cutaneous malignant melanoma is associated with distinct expression profiles: a tissue microarray-based study. Am J Pathol. 164: 193-203.

Anders, S., D. J. McCarthy, Y. Chen, M. Okoniewski, G. K. Smyth, W. Huber, and M. D. Robinson. (2013) Count-based differential expression analysis of RNA sequencing data using R and Bioconductor. Nat Protoc. 8: 1765-86.

Arora, A., and E. M. Scholar. (2005) Role of tyrosine kinase inhibitors in cancer therapy. J Pharmacol Exp Ther. 315: 971-9.

Arvind, R., H. Shimamoto, F. Momose, T. Amagasa, K. Omura, and N. Tsuchida. (2005) A mutation in the common docking domain of ERK2 in a human cancer cell line, which was associated with its constitutive phosphorylation. Int J Oncol. 27: 1499-504.

Benassi, B., M. Fanciulli, F. Fiorentino, A. Porrello, G. Chiorino, M. Loda, G. Zupi, and A. Biroccio. (2006) c-Myc phosphorylation is required for cellular response to oxidative stress. Mol Cell. 21: 509-19.

Bennasroune, A., A. Gardin, D. Aunis, G. Cremel, and P. Hubert. (2004) Tyrosine kinase receptors as attractive targets of cancer therapy. Crit Rev Oncol Hematol. 50: 23-38.

Boston, S. R., R. Deshmukh, S. Strome, U. D. Priyakumar, A. D. MacKerell, Jr., and P. Shapiro. (2011) Characterization of ERK docking domain inhibitors that induce apoptosis by targeting Rsk-1 and caspase-9. BMC cancer. 11: 7.

Burkhard, K. A., F. Chen, and P. Shapiro. (2011) Quantitative analysis of ERK2 interactions with substrate proteins: roles for kinase docking domains and activity in determining binding affinity. The Journal of biological chemistry. 286: 2477-85.

Carlton, J. G., A. Caballe, M. Agromayor, M. Kloc, and J. Martin-Serrano. (2012) ESCRT-III governs the Aurora B-mediated abscission checkpoint through CHMP4C. Science. 336: 220-5.

Cesi, G., G. Walbrecq, A. Zimmer, S. Kreis, and C. Haan. (2017) ROS production induced by BRAF inhibitor treatment rewires metabolic processes affecting cell growth of melanoma cells. Mol Cancer. 16: 102.

Chen, F., C. N. Hancock, A. T. Macias, J. Joh, K. Still, S. Zhong, A. D. MacKerell, Jr., and P. Shapiro. (2006) Characterization of ATP-independent ERK inhibitors identified through in silico analysis of the active ERK2 structure. Bioorg Med Chem Lett. 16: 6281-7.

Ciuffreda, L., D. Del Bufalo, M. Desideri, C. Di Sanza, A. Stoppacciaro, M. R. Ricciardi, S. Chiaretti, S. Tavolaro, B. Benassi, A. Bellacosa, R. Foa, A. Tafuri, F. Cognetti, A. Anichini, G. Zupi, and M. Milella. (2009) Growth-inhibitory and antiangiogenic activity of the MEK inhibitor PD0325901 in malignant melanoma with or without BRAF mutations. Neoplasia. 11: 720-31.

da Silva Almeida, A. C., F. Abate, H. Khiabanian, E. Martinez-Escala, J. Guitart, C. P. Tensen, M. H. Vermeer, R. Rabadan, A. Ferrando, and T. Palomero. (2015) The mutational landscape of cutaneous T cell lymphoma and Sezary syndrome. Nat Genet. 47: 1465-70.

Dayalan Naidu, S., and A. T. Dinkova-Kostova. (2020) KEAP1, a cysteine-based sensor and a drug target for the prevention and treatment of chronic disease. Open Biol. 10: 200105.

Defnet, A. E., W. Huang, S. Polischak, S. K. Yadav, M. A. Kane, P. Shapiro, and D. A. Deshpande. (2019a) Effects of ATP-competitive and function-selective ERK inhibitors on airway smooth muscle cell proliferation. FASEB J. 33: 10833-43.

———. (2019b) Effects of ATP-competitive and function-selective ERK inhibitors on airway smooth muscle cell proliferation. FASEB J: fj201900680R.

Dorfer, V., P. Pichler, T. Stranzl, J. Stadlmann, T. Taus, S. Winkler, and K. Mechtler. (2014) MS Amanda, a universal identification algorithm optimized for high accuracy tandem mass spectra. J Proteome Res. 13: 3679-84.

Drobic, B., B. Perez-Cadahia, J. Yu, S. K. Kung, and J. R. Davie. (2010) Promoter chromatin remodeling of immediate-early genes is mediated through H3 phosphorylation at either serine 28 or 10 by the MSK1 multi-protein complex. Nucleic Acids Res. 38: 3196-208.

Emery, C. M., K. G. Vijayendran, M. C. Zipser, A. M. Sawyer, L. Niu, J. J. Kim, C. Hatton, R. Chopra, P. A. Oberholzer, M. B. Karpova, L. E. MacConaill, J. Zhang, N. S. Gray, W. R. Sellers, R. Dummer, and L. A. Garraway. (2009) MEK1 mutations confer resistance to MEK and B-RAF inhibition. Proceedings of the National Academy of Sciences of the United States of America. 106: 20411-6.

Eng, J. K., B. Fischer, J. Grossmann, and M. J. Maccoss. (2008) A fast SEQUEST cross correlation algorithm. J Proteome Res. 7: 4598-602.

Erde, J., R. R. Loo, and J. A. Loo. (2014) Enhanced FASP (eFASP) to increase proteome coverage and sample recovery for quantitative proteomic experiments. J Proteome Res. 13: 1885-95.

Fedorenko, I. V., G. T. Gibney, V. K. Sondak, and K. S. Smalley. (2015) Beyond BRAF: where next for melanoma therapy? British journal of cancer. 112: 217-26.

Flaherty, K. T., and G. McArthur. (2010) BRAF, a target in melanoma: implications for solid tumor drug development. Cancer. 116: 4902-13.

Galadari, S., A. Rahman, S. Pallichankandy, and F. Thayyullathil. (2017) Reactive oxygen species and cancer paradox: To promote or to suppress? Free Radic Biol Med. 104: 144-64.

Gao, P., I. Tchernyshyov, T. C. Chang, Y. S. Lee, K. Kita, T. Ochi, K. I. Zeller, A. M. De Marzo, J. E. Van Eyk, J. T. Mendell, and C. V. Dang. (2009) c-Myc suppression of miR-23a/b enhances mitochondrial glutaminase expression and glutamine metabolism. Nature. 458: 762-5.

Germann, U. A., B. F. Furey, W. Markland, R. R. Hoover, A. M. Aronov, J. J. Roix, M. Hale, D. M. Boucher, D. A. Sorrell, G. Martinez-Botella, M. Fitzgibbon, P. Shapiro, M. J. Wick, R. Samadani, K. Meshaw, A. Groover, G. DeCrescenzo, M. Namchuk, C. M. Emery, S. Saha, and D. J. Welsch. (2017) Targeting the MAPK Signaling Pathway in Cancer: Promising Preclinical Activity with the Novel Selective ERK1/2 Inhibitor BVD-523 (ulixertinib). Mol Cancer Ther.

Goodman, M., R. M. Bostick, O. Kucuk, and D. P. Jones. (2011) Clinical trials of antioxidants as cancer prevention agents: past, present, and future. Free Radic Biol Med. 51: 1068-84.

Guan, C., L. He, Z. Chang, X. Gu, J. Liang, and R. Liu. (2020) ZNF774 is a potent suppressor of hepatocarcinogenesis through dampening the NOTCH2 signaling. Oncogene. 39: 1665-80.

Hancock, C. N., A. Macias, E. K. Lee, S. Y. Yu, A. D. Mackerell, Jr., and P. Shapiro. (2005) Identification of novel extracellular signal-regulated kinase docking domain inhibitors. J Med Chem. 48: 4586-95.

Haq, R., J. Shoag, P. Andreu-Perez, S. Yokoyama, H. Edelman, G. C. Rowe, D. T. Frederick, A. D. Hurley, A. Nellore, A. L. Kung, J. A. Wargo, J. S. Song, D. E. Fisher, Z. Arany, and H. R. Widlund. (2013) Oncogenic BRAF regulates oxidative metabolism via PGC1alpha and MITF. Cancer Cell. 23: 302-15.

Hochberg, Yoav Benjamini and Yosef. (1995) Controlling the False Discovery Rate: A Practical and Powerful Approach to Multiple Testing Journal of the Royal Statistical Society. Series B (Methodological). 57: 289-300.

Hu, J., H. Yao, F. Gan, A. Tokarski, and Y. Wang. (2012) Interaction of OKL38 and p53 in regulating mitochondrial structure and function. PloS one. 7: e43362.

Johannessen, C. M., J. S. Boehm, S. Y. Kim, S. R. Thomas, L. Wardwell, L. A. Johnson, C. M. Emery, N. Stransky, A. P. Cogdill, J. Barretina, G. Caponigro, H. Hieronymus, R. R. Murray, K. Salehi-Ashtiani, D. E. Hill, M. Vidal, J. J. Zhao, X. Yang, O. Alkan, S. Kim, J. L. Harris, C. J. Wilson, V. E. Myer, P. M. Finan, D. E. Root, T. M. Roberts, T. Golub, K. T. Flaherty, R. Dummer, B. L. Weber, W. R. Sellers, R. Schlegel, J. A. Wargo, W. C. Hahn, and L. A. Garraway. (2010) COT drives resistance to RAF inhibition through MAP kinase pathway reactivation. Nature. 468: 968-72.

Kall, L., J. D. Canterbury, J. Weston, W. S. Noble, and M. J. MacCoss. (2007) Semi-supervised learning for peptide identification from shotgun proteomics datasets. Nat Methods. 4: 923-5.

Kaoud, T. S., W. H. Johnson, N. D. Ebelt, A. Piserchio, D. Zamora-Olivares, S. X. Van Ravenstein, J. R. Pridgen, R. Edupuganti, R. Sammons, M. Cano, M. Warthaka, M. Harger, C. D. J. Tavares, J. Park, M. F. Radwan, P. Ren, E. V. Anslyn, K. Y. Tsai, R. Ghose, and K. N. Dalby. (2019) Modulating multi-functional ERK complexes by covalent targeting of a recruitment site in vivo. Nat Commun. 10: 5232.

Kerkhoff, E., R. Houben, S. Loffler, J. Troppmair, J. E. Lee, and U. R. Rapp. (1998) Regulation of c-myc expression by Ras/Raf signalling. Oncogene. 16: 211-6.

Korkut, A., W. Wang, E. Demir, B. A. Aksoy, X. Jing, E. J. Molinelli, O. Babur, D. L. Bemis, S. Onur Sumer, D. B. Solit, C. A. Pratilas, and C. Sander. (2015) Perturbation biology nominates upstream-downstream drug combinations in RAF inhibitor resistant melanoma cells. Elife. 4.

Kramer, A., J. Green, J. Pollard, Jr., and S. Tugendreich. (2014) Causal analysis approaches in Ingenuity Pathway Analysis. Bioinformatics. 30: 523-30.

Kunz, M., S. Moeller, D. Koczan, P. Lorenz, R. H. Wenger, M. O. Glocker, H. J. Thiesen, G. Gross, and S. M. Ibrahim. (2003) Mechanisms of hypoxic gene regulation of angiogenesis factor Cyr61 in melanoma cells. J Biol Chem. 278: 45651-60.

Lee, S., M. Warthaka, C. Yan, T. S. Kaoud, P. Ren, and K. N. Dalby. (2011) Examining docking interactions on ERK2 with modular peptide substrates. Biochemistry. 50: 9500-10.

Li, R., W. Chen, R. Yanes, S. Lee, and J. A. Berliner. (2007) OKL38 is an oxidative stress response gene stimulated by oxidized phospholipids. J Lipid Res. 48: 709-15.

MacDonald, G., I. Nalvarte, T. Smirnova, M. Vecchi, N. Aceto, A. Dolemeyer, A. Frei, S. Lienhard, J. Wyckoff, D. Hess, J. Seebacher, J. J. Keusch, H. Gut, D. Salaun, G. Mazzarol, D. Disalvatore, M. Bentires-Alj, P. P. Di Fiore, A. Badache, and N. E. Hynes. (2014) Memo is a copper-dependent redox protein with an essential role in migration and metastasis. Sci Signal. 7: ra56.

Madan, E., R. Gogna, P. Kuppusamy, M. Bhatt, A. A. Mahdi, and U. Pati. (2013) SCO2 induces p53-mediated apoptosis by Thr845 phosphorylation of ASK-1 and dissociation of the ASK-1-Trx complex. Mol Cell Biol. 33: 1285-302.

Mahalingam, M., R. Arvind, H. Ida, A. K. Murugan, M. Yamaguchi, and N. Tsuchida. (2008) ERK2 CD domain mutation from a human cancer cell line enhanced anchorage-independent cell growth and abnormality in Drosophila. Oncol Rep. 20: 957-62.

Maik-Rachline, G., and R. Seger. (2016) The ERK cascade inhibitors: Towards overcoming resistance. Drug Resist Updat. 25: 1-12.

Meierjohann, S. (2014) Oxidative stress in melanocyte senescence and melanoma transformation. Eur J Cell Biol. 93: 36-41.

Mendelsohn, J., and J. Baselga. (2006) Epidermal growth factor receptor targeting in cancer. Semin Oncol. 33: 369-85.

Mi, H., X. Huang, A. Muruganujan, H. Tang, C. Mills, D. Kang, and P. D. Thomas. (2017) PANTHER version 11: expanded annotation data from Gene Ontology and Reactome pathways, and data analysis tool enhancements. Nucleic Acids Res. 45: D183-D89.

Milde-Langosch, K. (2005) The Fos family of transcription factors and their role in tumourigenesis. Eur J Cancer. 41: 2449-61.

Morris, E. J., S. Jha, C. R. Restaino, P. Dayananth, H. Zhu, A. Cooper, D. Carr, Y. Deng, W. Jin, S. Black, B. Long, J. Liu, E. Dinunzio, W. Windsor, R. Zhang, S. Zhao, M. H. Angagaw, E. M. Pinheiro, J. Desai, L. Xiao, G. Shipps, A. Hruza, J. Wang, J. Kelly, S. Paliwal, X. Gao, B. S. Babu, L. Zhu, P. Daublain, L. Zhang, B. A. Lutterbach, M. R. Pelletier, U. Philippar, P. Siliphaivanh, D. Witter, P. Kirschmeier, W. R. Bishop, D. Hicklin, D. G. Gilliland, L. Jayaraman, L. Zawel, S. Fawell, and A. A. Samatar. (2013) Discovery of a novel ERK inhibitor with activity in models of acquired resistance to BRAF and MEK inhibitors. Cancer Discov. 3: 742-50.

Muller, J. M., M. A. Cahill, R. A. Rupec, P. A. Baeuerle, and A. Nordheim. (1997) Antioxidants as well as oxidants activate c-fos via Ras-dependent activation of extracellular-signal-regulated kinase 2 and Elk-1. Eur J Biochem. 244: 45-52.

Okazaki, K., T. Papagiannakopoulos, and H. Motohashi. (2020) Metabolic features of cancer cells in NRF2 addiction status. Biophys Rev. 12: 435-41.

Olayanju, A., I. M. Copple, H. K. Bryan, G. T. Edge, R. L. Sison, M. W. Wong, Z. Q. Lai, Z. X. Lin, K. Dunn, C. M. Sanderson, A. F. Alghanem, M. J. Cross, E. C. Ellis, M. Ingelman-Sundberg, H. Z. Malik, N. R. Kitteringham, C. E. Goldring, and B. K. Park. (2015) Brusatol provokes a rapid and transient inhibition of Nrf2 signaling and sensitizes mammalian cells to chemical toxicity-implications for therapeutic targeting of Nrf2. Free Radic Biol Med. 78: 202-12.

Piskounova, E., M. Agathocleous, M. M. Murphy, Z. Hu, S. E. Huddlestun, Z. Zhao, A. M. Leitch, T. M. Johnson, R. J. DeBerardinis, and S. J. Morrison. (2015) Oxidative stress inhibits distant metastasis by human melanoma cells. Nature. 527: 186-91.

Polsky, D., and C. Cordon-Cardo. (2003) Oncogenes in melanoma. Oncogene. 22: 3087-91.

Poulikakos, P. I., and N. Rosen. (2011) Mutant BRAF melanomas--dependence and resistance. Cancer Cell. 19: 11-5.

Poulikakos, P. I., and D. B. Solit. (2011) Resistance to MEK inhibitors: should we co-target upstream? Sci Signal. 4: pe16.

Pratilas, C. A., B. S. Taylor, Q. Ye, A. Viale, C. Sander, D. B. Solit, and N. Rosen. (2009) (V600E)BRAF is associated with disabled feedback inhibition of RAF-MEK signaling and elevated transcriptional output of the pathway. Proc Natl Acad Sci U S A. 106: 4519-24.

Preston, G. A., T. T. Lyon, Y. Yin, J. E. Lang, G. Solomon, L. Annab, D. G. Srinivasan, D. A. Alcorta, and J. C. Barrett. (1996) Induction of apoptosis by c-Fos protein. Mol Cell Biol. 16: 211-8.

Qi, D., P. Brownridge, D. Xia, K. Mackay, F. F. Gonzalez-Galarza, J. Kenyani, V. Harman, R. J. Beynon, and A. R. Jones. (2012) A software toolkit and interface for performing stable isotope labeling and top3 quantification using Progenesis LC-MS. OMICS. 16: 489-95.

Ren, D., N. F. Villeneuve, T. Jiang, T. Wu, A. Lau, H. A. Toppin, and D. D. Zhang. (2011) Brusatol enhances the efficacy of chemotherapy by inhibiting the Nrf2-mediated defense mechanism. Proc Natl Acad Sci U S A. 108: 1433-8.

Reuter, C. W., M. A. Morgan, and L. Bergmann. (2000) Targeting the Ras signaling pathway: a rational, mechanism-based treatment for hematologic malignancies? Blood. 96: 1655-69.

Samadani, R., J. Zhang, A. Brophy, T. Oashi, U. D. Priyakumar, E. P. Raman, F. J. St John, K. Y. Jung, S. Fletcher, E. Pozharski, A. D. MacKerell, Jr., and P. Shapiro. (2015) Small-molecule inhibitors of ERK-mediated immediate early gene expression and proliferation of melanoma cells expressing mutated BRaf. Biochem J. 467: 425-38.

Sammons, R. M., N. A. Perry, Y. Li, E. J. Cho, A. Piserchio, D. P. Zamora-Olivares, R. Ghose, T. S. Kaoud, G. Debevec, C. Bartholomeusz, V. V. Gurevich, T. M. Iverson, M. Giulianotti, R. A. Houghten, and K. N. Dalby. (2019) A Novel Class of Common Docking Domain Inhibitors That Prevent ERK2 Activation and Substrate Phosphorylation. ACS Chem Biol. 14: 1183-94.

Santini, R., S. Pietrobono, S. Pandolfi, V. Montagnani, M. D'Amico, J. Y. Penachioni, M. C. Vinci, L. Borgognoni, and B. Stecca. (2014) SOX2 regulates self-renewal and tumorigenicity of human melanoma-initiating cells. Oncogene. 33: 4697-708.

Sassone-Corsi, P., C. A. Mizzen, P. Cheung, C. Crosio, L. Monaco, S. Jacquot, A. Hanauer, and C. D. Allis. (1999) Requirement of Rsk-2 for epidermal growth factor-activated phosphorylation of histone H3. Science. 285: 886-91.

Shah, N. G., M. E. Tulapurkar, A. Ramarathnam, A. Brophy, R. Martinez, 3rd, K. Hom, T. Hodges, R. Samadani, I. S. Singh, A. D. MacKerell, Jr., P. Shapiro, and J. D. Hasday. (2017) Novel Noncatalytic Substrate-Selective p38alpha-Specific MAPK Inhibitors with Endothelial-Stabilizing and Anti-Inflammatory Activity. J Immunol. 198: 3296-306.

Shapiro, P. (2002) Ras-MAP kinase signaling pathways and control of cell proliferation: relevance to cancer therapy. Crit Rev Clin Lab Sci. 39: 285-330.

Shaw, P. E., and J. Saxton. (2003) Ternary complex factors: prime nuclear targets for mitogen-activated protein kinases. Int J Biochem Cell Biol. 35: 1210-26.

Shin, S. Y., Y. Y. Bahk, J. Ko, I. Y. Chung, Y. S. Lee, J. Downward, H. Eibel, P. M. Sharma, J. M. Olefsky, Y. H. Kim, B. Lee, and Y. H. Lee. (2006) Suppression of Egr-1 transcription through targeting of the serum response factor by oncogenic H-Ras. Embo J. 25: 1093-103.

Singh, A., S. Venkannagari, K. H. Oh, Y. Q. Zhang, J. M. Rohde, L. Liu, S. Nimmagadda, K. Sudini, K. R. Brimacombe, S. Gajghate, J. Ma, A. Wang, X. Xu, S. A. Shahane, M. Xia, J. Woo, G. A. Mensah, Z. Wang, M. Ferrer, E. Gabrielson, Z. Li, F. Rastinejad, M. Shen, M. B. Boxer, and S. Biswal. (2016) Small Molecule Inhibitor of NRF2 Selectively Intervenes Therapeutic Resistance in KEAP1-Deficient NSCLC Tumors. ACS Chem Biol. 11: 3214-25.

Singh, J., R. C. Petter, T. A. Baillie, and A. Whitty. (2011) The resurgence of covalent drugs. Nat Rev Drug Discov. 10: 307-17.

Sunryd, J. C., B. Cheon, J. B. Graham, K. M. Giorda, R. A. Fissore, and D. N. Hebert. (2014) TMTC1 and TMTC2 are novel endoplasmic reticulum tetratricopeptide repeat-containing adapter proteins involved in calcium homeostasis. J Biol Chem. 289: 16085-99.

Taus, T., T. Kocher, P. Pichler, C. Paschke, A. Schmidt, C. Henrich, and K. Mechtler. (2011) Universal and confident phosphorylation site localization using phosphoRS. J Proteome Res. 10: 5354-62.

Telkoparan-Akillilar, P., S. Suzen, and L. Saso. (2019) Pharmacological Applications of Nrf2 Inhibitors as Potential Antineoplastic Drugs. Int J Mol Sci. 20.

Trachootham, D., J. Alexandre, and P. Huang. (2009) Targeting cancer cells by ROS-mediated mechanisms: a radical therapeutic approach? Nat Rev Drug Discov. 8: 579-91.

Tuma, R. S. (2011) Getting around PLX4032: studies turn up unusual mechanisms of resistance to melanoma drug. J Natl Cancer Inst. 103: 170-1, 77.

von Kriegsheim, A., D. Baiocchi, M. Birtwistle, D. Sumpton, W. Bienvenut, N. Morrice, K. Yamada, A. Lamond, G. Kalna, R. Orton, D. Gilbert, and W. Kolch. (2009) Cell fate decisions are specified by the dynamic ERK interactome. Nat Cell Biol. 11: 1458-64.

Wang, L., R. Leite de Oliveira, S. Huijberts, E. Bosdriesz, N. Pencheva, D. Brunen, A. Bosma, J. Y. Song, J. Zevenhoven, G. T. Los-de Vries, H. Horlings, B. Nuijen, J. H. Beijnen, J. H. M. Schellens, and R. Bernards. (2018) An Acquired Vulnerability of Drug-Resistant Melanoma with Therapeutic Potential. Cell. 173: 1413-25 e14.

Webster, K. A., D. J. Discher, and N. H. Bishopric. (1994) Regulation of fos and jun immediate-early genes by redox or metabolic stress in cardiac myocytes. Circ Res. 74: 679-86.

Williamson, J. C., A. V. Edwards, T. Verano-Braga, V. Schwammle, F. Kjeldsen, O. N. Jensen, and M. R. Larsen. (2016) High-performance hybrid Orbitrap mass spectrometers for quantitative proteome analysis: Observations and implications. Proteomics. 16: 907-14.

Wisniewski, J. R., A. Zougman, N. Nagaraj, and M. Mann. (2009) Universal sample preparation method for proteome analysis. Nat Methods. 6: 359-62.

Wu, P., T. E. Nielsen, and M. H. Clausen. (2015) FDA-approved small-molecule kinase inhibitors. Trends Pharmacol Sci. 36: 422-39.

———. (2016) Small-molecule kinase inhibitors: an analysis of FDA-approved drugs. Drug Discov Today. 21: 5-10.

Yeh, T. C., V. Marsh, B. A. Bernat, J. Ballard, H. Colwell, R. J. Evans, J. Parry, D. Smith, B. J. Brandhuber, S. Gross, A. Marlow, B. Hurley, J. Lyssikatos, P. A. Lee, J. D. Winkler, K. Koch, and E. Wallace. (2007) Biological characterization of ARRY-142886 (AZD6244), a potent, highly selective mitogen-activated protein kinase kinase 1/2 inhibitor. Clin Cancer Res. 13: 1576-83.

Yuan, L., R. Mishra, H. Patel, S. Alanazi, X. Wei, Z. Ma, and J. T. Garrett. (2020) BRAF Mutant Melanoma Adjusts to BRAF/MEK Inhibitors via Dependence on Increased Antioxidant SOD2 and Increased Reactive Oxygen Species Levels. Cancers (Basel). 12.

Zhao, Z., and P. E. Bourne. (2018) Progress with covalent small-molecule kinase inhibitors. Drug Discov Today. 23: 727-35.

Zhong, H., and J. P. Bowen. (2011) Recent advances in small molecule inhibitors of VEGFR and EGFR signaling pathways. Curr Top Med Chem. 11: 1571-90.

Figure legends

Figure 1: Effects of **SF-3-026** and analogs on proliferation of cancer cell lines. Data show percent proliferation compared to controls (100%) for A375, RPMI7951, SK-Mel-28, HL-60, HeLa or Jurkat cells following treatment with 100 µM of each test compound for 48 hours. The mean and standard deviation from three independent experiments are shown.

Figure 2. SF-3-030 interacts with and modifies ERK2 via cysteine adduct formation. (**A**) Putative mechanisms of **SF-3-030** adduct formation with cysteine residues on ERK2. (**B**) Space-filling model of ERK2 with highlighted cysteine residues and **SF-3-030** modification site (adapted from PDB ID: 4GT3). Cysteine modifications determined by high-resolution liquid chromatography-tandem mass spectrometry. Cysteine residues are colored in (green), as well as the TXY motif (magenta), the F recruitment site (red), and the primary modification site C252 (red font).

Figure 3. Lead compounds differentially regulate IEG levels in A375 cells. (**A**) Immunoblots for c-Fos, c-Jun, FosB/B2, Fra1, and c-Myc proteins in cells treated with 10 µM SCH77294 or 25 µM **SF-3-030** for 0 – 24 hours. (**B**) Phosphorylated (S383) and total Elk-1 levels in cells treated with 10 µM SCH77294 or 25 µM **SF-3-030** for 0 – 24 hours. (**C**) Cells treated for 4 hours with varying doses of **SF-2-110**, **SF-3-026**, or **SF-3-030**. Controls include untreated or cells treated with 5 µM AZD6244 or SCH772984. Immunoblots show relative c-Fos, c-Jun, FosB/B2, Fra1, and c-Myc protein levels. Levels of active ERK1/2 (ppERK1/2), total ERK2, and α-tubulin are shown to demonstrate ERK1/2 pathway activity and equal protein loading in (**A**) and (**C**). (**D**) Relative quantification of c-Fos, Fra-1, and c-Myc protein levels after 4 hour exposure with 25µM of **SF-2-110** or **SF-3-030.** Mean and STD are from three independent experiments and graph was determined via densitometry as described in the Methods. * and ** represent p<0.05

and p<0.01, respectively. (**E**) A375 cells were exposed to **SF-3-030** for the indicated times and then incubated with fresh media without compound for a total incubation time of 24 hours. Lysates were immunoblotted for cleaved PARP, phosphorylated histone H3 (pH3) and total ERK2 for a loading control. Data are representative of three independent experiments. The numbers in each immunoblot represent the relative levels of protein, normalized to α-tubulin, as determined by densitometry. Molecular weight markers (kDa) are indicated on the right of each immunoblot.

Figure 4. SF-3-030 induces NRF2 levels. (**A**) Immunoblot analysis of NRF2 in A375 cells treated with 10 μM SCH772984 or 25 μM **SF-3-030** for 0-24 hours. (**B**) NRF2 levels in A375 cells treated with 25 μM **SF-3-030** plus or minus 5 mM N-acetyl cysteine (NAC) for 0, 1, or 4 hours. Non-specific bands that cross-react with the NRF2 primary antibody are indicated (ns) for panels **A** and **B**. The graph in panel **C** shows the densitometry quantitation of NRF2 under the conditions described in (**B**). Mean and STD are from three independent experiments. *indicates statistical significance compared to **SF-3-030** treatment only (p<0.05). The numbers in each immunoblot represent the relative levels of protein, normalized to α-tubulin, as determined by densitometry. Molecular weight markers are indicated on the left of each immunoblot.

Figure 5. SF-3-030 induction of ROS mediates inhibition of A375 cell proliferation. (**A**) ROS was measured by CellROX Deep red reagent fluorescence in A375 cells treated with 25 μM **SF-3-030** in the absence (white bars) or presence (black bars) of the following ROS inhibitors (ROSi); 10 mM sodium pyruvate (Na Pyr), 100 mM mannitol (Mann), or 10 mM N-acetyl cysteine (NAC) for 60 minutes. Graphs represent three independent experiments and each data point represents the average ± STD from 3 wells with 4 fields of view per well, with each field containing between 500-1000 cells. Statistical significance was determined within each

40

experiment (* and ** represent $p<0.05$ and $p<0.01$, respectively). (**B**) A375 cell viability was measured after 48 hours in untreated or **SF-3-030** treated cells in the absence (white bars) or presence (black bars) of the ROS inhibitors at the concentrations described in panel **A**. The mean and STD for cell proliferation are from three independent experiments. ** indicates statistical significance ($p<0.01$) compared to **SF-3-030** treatment only. (**C**) Relative levels of c-Fos after 4 hours treatment with **SF-3-030** alone (white bars) or in combination with the indicated ROS inhibitors (black bars) at the concentrations indicated in panel **A**. Relative c-Fos levels were determined by ProteinSimple immunoanalysis and normalized to total β-actin.

Figure 6. NRF2 inhibitors do not affect **SF-3-030** inhibition of A375 cell proliferation. (**A**) A375 cells were treated for 8 hours with 25 μM **SF-3-030** in the absence or presence of ML-385 (50 μM) or brusatol (Bru; 30 nM). Lysates were immunoblotted for relative levels of NRF2, NQO1, HMOX-1 and OSGIN1 as shown. (**B**) A375 lysates from cells treated for 8 hours with 25 μM **SF-3-030 (SF)** in the absence or presence of brusatol (Bru; 30 nM), were immunoblotted for GCLM and SRXN1. Positive control lysates from HeLa and A549 cells were used for GCLM and SRXN1, respectively. The numbers in each immunoblot represent the relative levels of protein, normalized to ß-actin, as determined by densitometry. Molecular weight markers are indicated on the left of each immunoblot. (**C**) A375 cell viability with varying doses of ML-385 or (**D**) brusatol. (**E**) Cell viability with varying doses of **SF-3-030** in the absence (white bars) or presence (black bars) of 50 μM ML-385. (**F**) Combination index with varying doses of **SF-3-030** and brusatol. Untreated control cells are indicated with a striped column. Relative cell viability was measured after 48 hours and data are representative of three independent experiments.

Table 1. High-resolution liquid chromatography-tandem mass spectrometry analysis of proteins

that increase or decrease ≥1.5 fold following treatment with **SF-3-030 (A)** or SCH772984 **(B)** for

4 hours relative to untreated A375 cells (set at 1). Protein changes common to both **SF-3-030** and

SCH772984 are *italicized*.

A.

Proteins that increase with SF-3-030	fold increase
Zinc finger protein 774 (ZNF774)	16.28
Mediator of cell motility 1 (MEMO1)	10.55
Chromosome 18 open reading frame 17 isoform CRA c (TTC39C)	5.18
Unconventional myosin-XVIIIa (MYO18A)	4.18
Transcription factor 4 (TCF4)	2.24
Heme oxygenase 1 (HMOX1)	1.77
Proteins that decrease with SF-3-030	**fold decrease**
Cytochrome c-type heme lyase (HCCS)	3.35
Uncharacterized protein KIAA1211 (KIAA1211)	2.24
Alpha-actinin-2 (ACTN2)	1.66
Adenosylhomocysteinase (AHCY)	*1.53*

B.

Proteins that increase with SCH772984	fold increase
Transmembrane and TPR repeat-containing protein 1 (TMTC1)	5.15
SLIT-ROBO Rho GTPase-activating protein 1 (SRGAP1)	1.47
Proteins that decrease with SCH772984	**fold decrease**
Tetratricopeptide repeat protein 29 (TTC29)	2.44
Adenosylhomocysteinase (AHCY)	*1.48*

Table 2: High-resolution liquid chromatography-tandem mass spectrometry analysis of proteins that increase or decrease ≥1.5 fold following treatment with **SF-3-030 (A)** or SCH772984 **(B)** for 12 hours relative to untreated A375 cells (set at 1). Protein changes common to both **SF-3-030** and SCH772984 are *italicized*.

A.

Proteins that increase with SF-3-030	fold increase
Oxidative stress-induced growth inhibitor 1 (OSGIN1)	21.04
Zinc finger protein 774 (ZNF774)	18.18
Transcription factor 4 (TCF4)	*10.95*
Peroxidasin homolog (PXDN)	9.43
Protein MEMO1 (MEMO1)	8.37
Chromosome 18 open reading frame 17_isoform CRA_c (TTC39C)	7.31
Unconventional myosin-XVIIIa (MYO18A)	4.50
Protein SCO2 homolog mitochondrial (SCO2)	*3.89*
Jouberin (AHI1)	3.12
Heme oxygenase 1 (HMOX1)	3.02
Protein moonraker (KIAA0753)	2.26
Ankyrin repeat and SOCS box protein 6 (ASB6)	2.07
RalBP1-associated Eps domain-containing protein 1 (REPS1)	1.98
Nucleolar complex protein 2 homolog (NOC2L)	1.73
Sickle tail protein homolog (KIAA1217)	1.71
Condensin-2 complex subunit D3 (NCAPD3)	1.49
Proteins that decrease with SF-3-030	**fold decrease**
Myomegalin (PDE4DIP)	2.80
Cytochrome c-type heme lyase (HCCS)	2.49
AP-1 complex subunit mu-1 (AP1M1)	2.24
Cyclic nucleotide-gated cation channel beta-1 (CNGB1)	2.11
Forkhead box protein R2 (FOXR2)	1.76
Glutamate receptor-interacting protein 2 (GRIP2)	1.72
SUN domain-containing protein 1 (Fragment) (SUN1)	1.68
Probable ribosome biogenesis protein RLP24 (RSL24D1)	*1.66*
Uncharacterized protein KIAA1211 (KIAA1211)	*1.62*
Integrator complex subunit 2 (INTS2)	1.51

B.

Proteins that increase with SCH772984	fold increase
Forkhead box protein D3 (FOXD3)	32.88
Plakophilin-2 (PKP2)	4.76
Polyadenylate-binding protein 3 (PABPC3)	2.85
WD repeat-containing protein 59 (WDR59)	2.76
Protein SCO2 homolog mitochondrial (SCO2)	*2.69*
Transcription factor 4 (TCF4)	*2.64*
Uncharacterized protein KIAA1211 (KIAA1211)	*1.84*
HBS1-like protein (HBS1L)	1.71
Protein disulfide-isomerase A3 (Fragment) (PDIA3)	1.61
Glutamine--fructose-6-phosphate aminotransferase 2 (GFPT2)	1.48
Proteins that decrease with SCH772984	**fold decrease**
Voltage-dependent L-type calcium channel subunit beta-4 (CACNB4)	2.65
Phosphodiesterase 5A cGMP-specific isoform CRA_a (PDE5A)	2.18
Replication factor C subunit 4 (RFC4)	2.08
mRNA cap guanine-N7 methyltransferase (RNMT)	1.88
Probable phospholipid-transporting ATPase IH (ATP11A)	1.82
Transcription factor AP-2-alpha (TFAP2A)	1.74
Probable ribosome biogenesis protein RLP24 (RSL24D1)	*1.70*
Decorin (DCN)	1.68
Hexokinase-2 (HK2)	1.60
1-acylglycerol-3-phosphate O-acyltransferase ABHD5 (ABHD5)	1.59
Collagen alpha-1(I) chain (COL1A1)	1.48

Figure 1
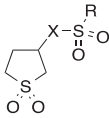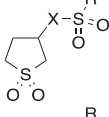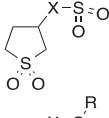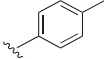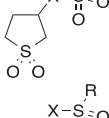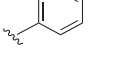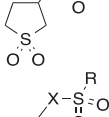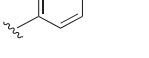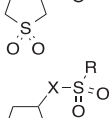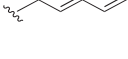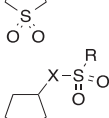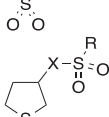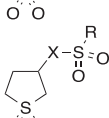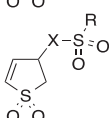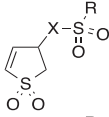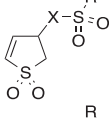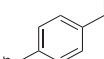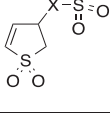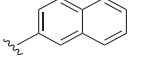
Code Number	Structure	X	R	Cell Viability (% of vehicle)					
				A375	RPMI-7951	SK-MEL-28	HL-60	HeLa	Jurkat
SF-2-110		O		115 ± 3	98 ± 7	99 ± 4	103 ± 36	97 ± 6	104 ± 2
SF-3-006		NMe		105 ± 1	98 ± 6	96 ± 6	98 ± 13	96 ± 6	97 ± 4
SF-3-007		NMe		102 ± 2	91 ± 2	93 ± 5	76 ± 17	92 ± 1	79 ± 2
SF-3-008		NMe		86 ± 1	100 ± 4	93 ± 5	64 ± 31	80 ± 2	75 ± 9
SF-3-009		NMe		98 ± 4	67 ± 3	90 ± 6	88 ± 26	85 ± 4	97 ± 4
SF-3-010		NMe		112 ± 5	117 ± 9	84 ± 7	99 ± 33	78 ± 5	79 ± 3
SF-3-011		NH		102 ± 3	110 ± 1	98 ± 7	131 ± 49	90 ± 5	97 ± 2
SF-3-013		NBn		106 ± 1	105 ± 4	94 ± 3	89 ± 20	86 ± 6	86 ± 2
SF-3-017		NEt		111 ± 5	105 ± 6	98 ± 5	97 ± 23	92 ± 7	94 ± 2
SF-3-018		N/Pr		106 ± 1	102 ± 9	93 ± 4	82 ± 20	88 ± 3	89 ± 2
SF-3-026		O		5.2 ± 1.0	0.10 ± 0.04	36 ± 13	0.4 ± 0.2	49 ± 7	64 ± 20
SF-3-027		O		5.1 ± 1.0	0.10 ± 0.04	6.9 ± 4.0	0.6 ± 0.2	26 ± 6	19 ± 7
SF-3-029		O		8.2 ± 1.0	0.20 ± 0.03	9.4 ± 5.0	1.8 ± 1.0	26 ± 4	35 ± 11
SF-3-030		O		4.9 ± 1.0	0.10 ± 0.03	26 ± 7	1.3 ± 0.3	52 ± 7	70 ± 12

Figure 2

A.
Substitution (S$_N$2' and S$_N$2)

M → M + 116

Michael Addition

M → M + 324

B.

Figure 3

Figure 4

A.

B.

C.

Figure 5

Figure 6